ACS APPLIED MATERIALS & INTERFACES

Research Article

www.acsami.org

Traps in Regioregular Poly(3-hexylthiophene) and its Blend with [6,6]-Phenyl-C_{61}-Butyric Acid Methyl Ester for Polymer Solar Cells

Cheng-Yen Yu, Tzu-Hao Jen, and Show-An Chen*

Chemical Engineering Department and Frontier Research Center on Fundamental and Applied Sciences of Matters, National Tsing-Hua University, No. 101, Section 2, Kuang-Fu Road, Hsinchu, Taiwan, 30013, Republic of China

ABSTRACT: Thermally stimulated current (TSC) technique is used to characterize traps in the regioregular poly(3-hexylthiophene) (rr-P3HT) and its blend with [6,6]-phenyl-C_{61}-butyric acid methyl ester (PCBM). A hole trap in bulk rr-P3HT and an interfacial hole trap located at indium tin oxide (ITO)/rr-P3HT interface are revealed from the TSC measurement. Besides, molecular oxygen (O_2) can form a deep electron trap with an onset of detrapping temperature at 225 K in rr-P3HT, in which O_2 is located at the main chain region and the detrapping process is induced by chain motions under elevated temperature. In the blend of rr-P3HT:PCBM (1:1 w/w), additional hole trap states are generated in this blend system as compared to those of pure rr-P3HT and PCBM; however, these hole trap states can be reduced by thermal or solvent annealing approaches. Similar to rr-P3HT, a deep electron trap with an onset of detrapping temperature at 250 K can be formed in the blend after O_2 exposure. In the case of low PCBM content in the blend (rr-P3HT:PCBM weight ratio of 4:1), an additional electron trap is generated.

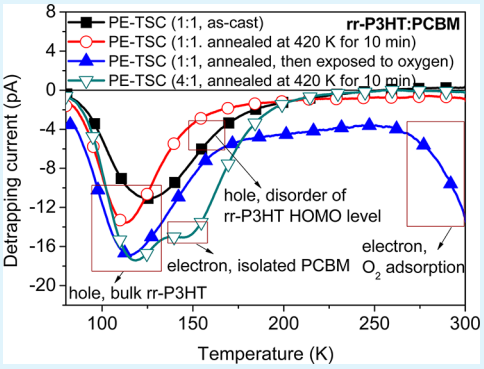

KEYWORDS: *poly(3-hexylthiophene), charge trap, thermally stimulated current, photovoltaic devices, [6,6]-phenyl-C_{61}-butyric acid methyl ester*

INTRODUCTION

Application of conjugated polymer to solar cells has attracted great attention due to the ease of fabrication, promising flexibility, and capability for large scale and low cost production. Recently, the power conversion efficiency (PCE) of state-of-the-art bulk heterojunction (BHJ) polymer solar cell (PSC) reaching 9.2% has been demonstrated using a conjugated polymers and a fullerene derivative as donor and acceptor materials,[1] showing its potential as a donor in photovoltaic devices. The regioregular poly(3-hexylthiophene) (rr-P3HT) and [6,6]-phenyl-C_{61}-butyric acid methyl ester (PCBM) are the most intensely investigated conjugated polymer donor material and acceptor material, respectively. PSCs based on these two materials can reach PCEs of 4−5%[2,3] and are considered as a model system for device physics studies for BHJ-PSCs.[4]

The thermally stimulated current (TSC) technique is one of the powerful methods for a determination of traps in the inorganic and organic materials.[5−9] In this technique, charge traps are filled using photoexitation (PE) at low temperature, by which charge carriers are generated directly in the bulk, or using field induction (FI) by which charge carriers are injected from the electrodes. Trapped charge carriers are then released by linearly increasing temperature, and the corresponding detrapping current against temperature is recorded taking as the TSC spectrum, from which information about traps in the material can be analyzed.

Although studies on traps in rr-P3HT and its blend with PCBM have been reported,[10−12] trap polarities and detrapping mechanism are still not clear yet. The presence of traps in the active layer can lead to a decrease in carrier mobility, generation of Joule heat by recombination of trapped charges with passing by opposite charges, and disturbance of the internal field distribution.[10,13,14] Thus, to identify the origins and states of traps is of fundamental importance in development of highly efficient PSCs. In this work, traps and their polarities in rr-P3HT and its blend with PCBM are investigated by a combination of PE-TSC and FI-TSC techniques. In addition, the influence of adsorbed molecular oxygen (O_2) on the traps and its detrapping process are also examined. We found that hole traps exist in bulk rr-P3HT and its interface with indium tin oxide (ITO); the molecular O_2 in bulk rr-P3HT can form a deep electron trap with an onset of detrapping temperature at 225 K. The detrapping process for trapped electrons is strongly related to main chain motion of rr-P3HT. In the blend of rr-P3HT with PCBM, both thermal and solvent annealing processes and blend ratio can have significant effects on distribution of trap states.

EXPERIMENTAL SECTION

Materials. rr-P3HT (catalog number: 4002-E) was supplied by Rieke Metals. PCBM (99.5% purity) was supplied by Nano-C. All materials were used as received.

Received: December 20, 2012
Accepted: March 19, 2013
Published: March 19, 2013

Sample Preparation. ITO glass substrates were cleaned sequentially with detergent aqueous solution, deionized water, acetone and isopropyl alcohol. The cleaned ITO glass was then treated with oxygen plasma at a pressure of 1.93×10^{-1} Torr for 5 min. A 20 nm thick poly(3,4-ethylenedioxythiophene):poly(styrenesulfonate) (PEDOT:PSS, Clevios P VP AI 4083 as aqueous solution) was spin-coated onto the treated ITO. After drying for 10 min at 140 °C in vacuum, a layer (330 nm) of rr-P3HT was spin-coated from its solution (40 mg mL^{-1}) in 1,2-dichlorobenzene (ODCB) on top of PEDOT:PSS and dried in a covered glass Petri dish for 1 h. In some cases, rr-P3HT was directly deposited onto ITO substrate from its solution in ODCB by spin-coating and dried in a covered glass Petri dish for 1 h (film thickness 330 nm) or by drop-casting and drying in a covered glass Petri dish for three days (film thickness 7 μm). For composite film, rr-P3HT and PCBM were dissolved in chlorobenzene (CB) with different blending ratios (1:1 and 4:1 by weight) at a total concentration of 40 mg mL^{-1}. Then, they were deposited onto the PEDOT:PSS-precoated ITO by spin-coating, resulting in film thickness of 260 and 290 nm, respectively. All the processes were carried out in a glovebox with argon, except those for ITO cleaning and PEDOT:PSS coating. Finally, a layer of Al (about 80 nm) as the cathode was deposited in a vacuum thermal evaporator through a shadow mask at a pressure of less than 2×10^{-6} Torr. The active area of the device is about 7 mm^2. All the thermal annealing treatments in this study were carried out after device fabrication.

TSC Measurement. For the TSC measurement, the device was mounted in a temperature-controlled, custom-built cryostat cooled with liquid nitrogen at a dynamic vacuum of less than 3×10^{-6} Torr. Trap filling was achieved by PE and FI methods. In the case of PE-TSC, the device was irradiated by a 75 W xenon lamp at 80 K for 5 min. The generated charge carriers were separated by the built-in electric field and captured by traps. In the case of FI-TSC, the different electric fields were applied to the device for 5 min at 80 K. For both PE-TSC and FI-TSC, after a dwell time of 15 min for the charge carriers to reach thermal equilibrium, the device was then heated at a constant rate of 10 K min^{-1} to 300 K with zero bias while recording the current by source-measure unit Keithley 236, by which detrapped charge carriers were extracted from the device only by the built-in voltage. Afterward, the device was successively cooled down to initial temperature 78 K and heated to 300 K again with a constant heating rate 10 K min^{-1} to record the dark current. Then, all the trap release currents were subtracted by their corresponding dark currents and then smoothed out by the adjacent-averaging method.

Depolarization Current Measurement. For depolarization current measurement, the device was polarized under an electric voltage for 5 min at 350 K and then cooled under this voltage to 78 K, at such low temperature the thermal energy is not sufficient for chain relaxation. The electric voltage was subsequently adjust to zero bias for 15 min so that the discharge current was reduced to a negligible level. The device was then heated at a constant rate of 10 K min^{-1} to 350 K with zero bias while recording the depolarization current due to chain relaxation.

RESULTS AND DISCUSSION

Traps in rr-P3HT. Figure 1 shows the PE-TSC spectra from 80 to 170 K for rr-P3HT without and with thermal annealing at 350 K for 30 min, for which rr-P3HT was spin-coated onto PEDOT:PSS-precoated ITO. The former (without annealing) exhibits a peak ranging from 80 to 170 K with a maximum at 118 K, and no additional TSC peak appears up to room temperature. The fluctuation after 170 K is caused by slight experimental deviation between the dark current and the detrapping current. Whereas the latter (with the thermal annealing) exhibits a slight shift toward lower temperature giving a maximum at 114 K, indicating that no new trap is generated and hence its bulk morphology does not change significantly after the thermal annealing process. This result can be explained as follows: the utilization of high-boiling-point solvent ODCB and slow drying of spin-coated film for rr-P3HT can improve the chains ordering of rr-P3HT as observed in the rr-P3HT:PCBM blend film.[2] As a result, it can be expected that bulk morphology of rr-P3HT (or chains ordering of rr-P3HT) and thus TSC spectrum does not change significantly after further thermal treatment. Besides, the broad TSC peak in PE-TSC spectra also suggests a distribution of trap states in the bulk rr-P3HT.

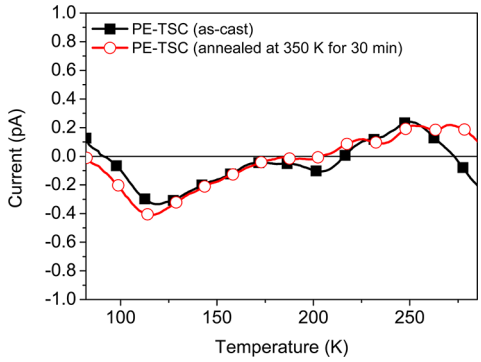

Figure 1. Comparison of PE-TSC spectra of a rr-P3HT device before and after annealing of the sample for 30 min at 350 K. The device structure is ITO/PEDOT:PSS(20 nm)/rr-P3HT(330 nm)/Al.

It has been shown that a much broader TSC peak between about 28 and 140 K (peak maximum at 85 K) was observed for rr-P3HT,[10] which is different from our result. This difference can be ascribed to different experimental condition involved. In our experiment, TSC measurement was performed in a liquid-nitrogen cooled cryostat with the trap filling at 80 K, while much lower trap-filling temperature (20 K) was employed in that study. As a result, the present TSC measurement actually can be regarded as the fractional TSC with trap-prerelease up to 80 K relative to the TSC with the low trap-filling temperature. Apart from this, there is still slight difference between our TSC result and the fractional TSC with T_{stop} = 80 K (T_{stop} is the preheating temperature) as reported in ref 10, in which the latter gives a broad TSC peak between about 72 and 130 K with the peak maximum at 92 K lower than that of the present case 114 K by 22 K. This discrepancy can be attributed to the higher film thickness in the present case (330 versus 220 nm) which results in a larger effective activation energy of trap due to a decreased Poole–Frenkel effect (field-reduction of the Coulombic potential barrier) in the former.[15] The faster heating rate of our TSC measurement (10 K min^{-1}) as compared to that (7 K min^{-1}) in ref 10 can also be a possible reason for the higher detrapping temperature.[16] All of the above discussions imply that our TSC spectrum originates from the same trap as that reported in the literature.

Effects of exposure to O_2 on PE-TSC of rr-P3HT were also investigated and corresponding PE-TSC results are shown in Figure 2a. For the thermally annealed sample exposing to dry O_2 for 12 h, its TSC peak height at 110 K is larger than that without O_2 exposure by the factor about 5, similar to that reported previously.[10] This result indicates that O_2 could lead to an increase in the trap density or more efficient trap filling due to promoted excition dissociation induced by O_2. The latter phenomenon can also be employed to explain the increase in detrapping current as we introduce an acceptor (PCBM) into pure rr-P3HT as will be discussed later. Since the PE-TSC spectrum can either be originated from hole or electron detrapping current, to identify polarities of the traps

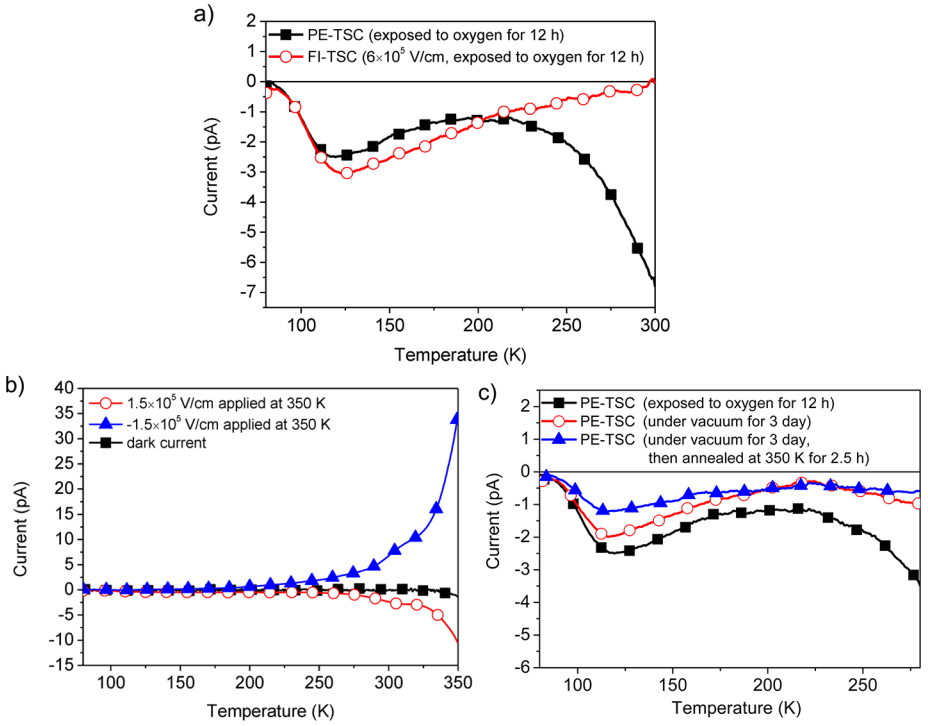

Figure 2. (a) PE-TSC and FI-TSC spectra of a rr-P3HT device after exposure to dry O_2 for 12 h. (b) Depolarization current measurement of a rr-P3HT device (device structure: ITO/rr-P3HT/Al). The measurement was carried out by applying positive and negative electric field 1.5×10^5 V cm^{-1} at 350 K for 5 min and freezing to 80 K quickly and then increasing the temperature at a rate of 10 K min^{-1}. (c) Effects of vacuum and thermal treatments on PE-TSC spectra of the rr-P3HT device after exposure to O_2.

are necessary. For doing so, trap filling with positive electric field 6×10^5 V cm^{-1} (corresponding to 6 V with film thickness 100 nm) was employed. The HOMO and LUMO levels of rr-P3HT are 5.2 and 3.3 eV, respectively,[17,18] along with the work functions of PEDOT:PSS (anode, 5.1 eV) and Al (cathode, 4.3 eV) involved in the device structure,[19,20] the barrier for hole injection (0.1 eV) is much lower than that for electron injection (1.0 eV) and thus the injected hole current for trap filling at 80 K is expected to be much higher than the injected electron current under this positive electric field. Consequently, a TSC peak contributed by hole current should appear after this electrical trap filling. As shown in Figure 2a, the FI-TSC spectrum has a peak at 120 K close to that in PE-TSC (110 K), thus this trap can be assigned to hole trap.

In the PE-TSC upon O_2 exposure, in addition to the growth of the TSC peak at 110 K, the detrapping current profile at temperature greater than 225 K grows rapidly with temperature (Figure 2a). However, the FI-TSC shows a gradual decay and leveling off at 300 K. The rapid rise of detrapping current above 225 K in PE-TSC indicates generation of additional deep electron trap in rr-P3HT upon O_2 exposure. The electron trap generated by adsorbed O_2 in rr-P3HT is found for the first time. In our previous work on poly[2-methoxy-5-(2′-ethyl-hexyloxy)-1,4-phenylene vinylene] (MEH-PPV),[21,22] we have successfully determined that high-electron-affinity O_2 can serve as an electron trap, in which O_2 is physically adsorbed in main chain region as evidenced by closely related temperatures for chain relaxation and detrapping current. For rr-P3HT, similar detrapping mechanism is proposed as follows. As O_2 diffuses into the bulk film of rr-P3HT, it is physically absorbed in the main chain region since the onset temperature of detrapping current at high-temperature region (T > 225 K) is close to that of the main chain relaxation of rr-P3HT (258−348 K with the glass transition temperature 300 K) as determined by the loss tangent (tan δ) of dynamic mechanical analysis (DMA).[23] As a result, when the temperature reaches the relaxation temperature of the main chain, chain motion starts and results in an oxygen desorption accompanied by a release of trapped electrons. The closely related temperatures between main chain relaxation and detrapping current can be further supported by measurement of depolarization current, which has been widely applied for nonconjugated polymers to investigate their chain relaxations.[24−26] Figure 2b shows the depolarization current spectra of rr-P3HT, which was obtained by polarization of the rr-P3HT device with positive and negative electric fields 1.5×10^5 V cm^{-1} for 5 min at 350 K, then freezing to 80 K quickly, and subsequently increasing the temperature to 350 K at a rate of 10 K min^{-1}. The two current profiles distributed from 230 to 350 K (with a transition point corresponding to glass transition at 310 K) appear to possess the same transitions as well as symmetry in magnitude (a characteristic of depolarization current) and can be attributed to depolarization of rr-P3HT main chain since it is close to main chain relaxation region of rr-P3HT determined by DMA. In comparison with electron detrapping current at high-temperature region (T > 225 K) in Figure 2a, it can be inferred that the released electron current is mainly contributed from the main chain relaxation of rr-P3HT.

Furthermore, these traps related to O_2 in rr-P3HT exhibit a partial reversibility in their charge trapping capability. By storing the sample in vacuum for 3 days, both trapped electrons and holes related to adsorbed O_2 can be significantly reduced due to the desorption of O_2 as shown in Figure 2c. The trapped charges can be further reduced by the thermal treatment (annealed at 350 K under vacuum for 2.5 h), since an enhanced chain motion of rr-P3HT at the temperature higher than the glass transition temperature (310 K) can lead to a further

desorption of O_2. However, this partial reversibility also indicates that it is not possible to totally eliminate the O_2 induced trapped charges in rr-P3HT. Therefore, it is very important to prevent rr-P3HT based devices from exposure to O_2 for avoiding any possible degradation in device performance resulting from a formation of new deep trap and promoted trapped charges.

An additional TSC peak ranging from 120 to 240 K with a maximum at 200 K has been reported previously in the case without PEDOT:PSS.[11] However, no such TSC peak was observed in the other work.[10] We compared these two works and found that there is no PEDOT:PSS layer in the former, but with it in the latter. Here we found that this TSC peak at 200 K can be attributed to a formation of interfacial trap at ITO/rr-P3HT interface as to be revealed below. Figure 3a shows the

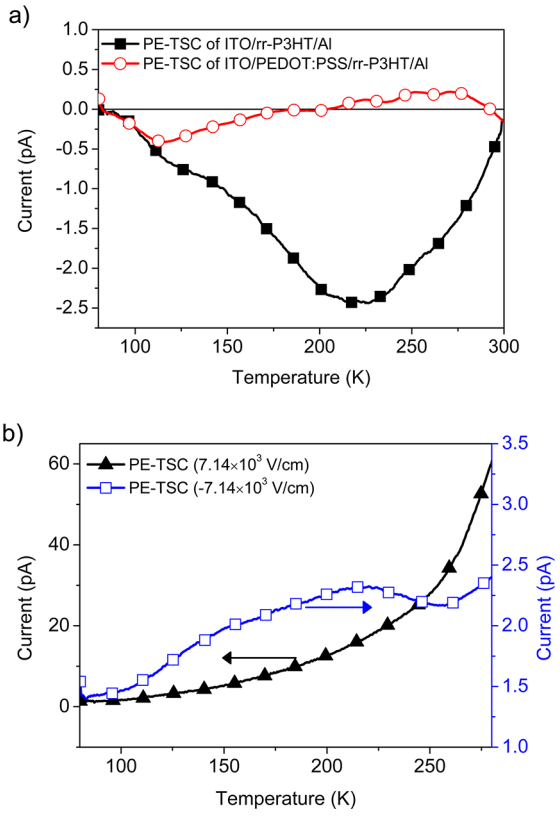

Figure 3. (a) PE-TSC spectra of spin-coating rr-P3HT with and without PEDOT:PSS as hole transport layer. (b) Absolute value of PE-TSC spectra for the drop-casting rr-P3HT (device structure ITO/rr-P3HT(7 μm)/Al) obtained after excitation at 78 K by the light at the absorption maximum (λ_{max} = 530 nm) from the ITO side under positive and negative drain electrical fields of 7.14 × 10^3 V cm^{-1}.

PE-TSC spectra for ITO/rr-P3HT/Al and the same device but with additional PEDOT:PSS layer as hole transport layer (ITO/PEDOT:PSS/rr-P3HT/Al). The latter is taken from the thermal annealed TSC in Figure 1, which, as discussed above, shows a PE-TSC peak ranging from 80 to 170 K with a maximum at 110 K. However, the former exhibits a main TSC peak at about 220 K (close to the TSC peak 200 K reported previously[11]) and a shoulder at about 110 K, which is at the same position as in the former device and should be originated from the same trap (hole trap). Since the TSC peak at 220 K can be eliminated by surface modification of ITO/rr-P3HT interface (that is, insertion of PEDOT:PSS between ITO and rr-P3HT); therefore, it can be rationally attributed to interfacial trap located at the ITO/rr-P3HT interface.

To further identify the polarity of the above interfacial trap, PE-TSC using the light at the λ_{max} of UV−vis absorption of rr-P3HT (530 nm) on a thick film (~7 μm) was employed. The excitation wavelength near λ_{max} can generate carriers "confined" in traps in the near-surface region about a few nanometers.[22] At elevated temperatures, the detrapped carriers can be collected by the vicinal electrode or drift through the sample to the counter electrode (i.e., traveling a longer distance) under an opposite drain field. A longer transporting distance will cause a time delay in the collection of carriers and thus result in TSC signals at higher temperature when heating at a constant rate. Therefore, the trap polarity can be assigned from the variation of TSC peak locations.[22] Figure 3b shows the PE-TSC (excitation wavelength 530 nm) for a 7-μm-thick rr-P3HT film under positive and negative drain electric fields of 7.14 × 10^3 V cm^{-1} (equivalent to 0.071 V for a film 100 nm thick by which will be no injected carriers) on the front electrode ITO, where the rr-P3HT film was coated on ITO glass substrates by drop casting from its solution in ODCB. In the case of positive bias, trap current increases significantly with temperature as T > 150 K. However, no distinct peak can be seen from the PE-TSC spectrum. When the drain voltage was altered to negative bias, the PE-TSC spectrum shows a peak at about 220 K. These results indicate that the interfacial trap at 220 K can be ascribed to a hole trap as discussed below. Under the positive bias, detrapped holes must drift through the polymer layer toward the counter electrode; therefore, these holes will be largely affected by carrier transport property of rr-P3HT, in which hole transport in rr-P3HT has been reported to be dispersive.[27] This dispersive transport for holes will lead to the finding that no distinct peak can be observed from the PE-TSC spectrum. On the other hand, detrapped holes are collected by the vicinal electrode ITO (i.e., travel a much shorter distance) under negative bias; as a result, hole transport is less affected by the bulk film of rr-P3HT and the TSC peak can be clearly observed from the TSC measurement.

The fact that the interfacial hole trap located at ITO/rr-P3HT vanishes by inserting PEDOT:PSS suggests that the hole collection layer (such as PEDOT:PSS) is necessary in the polymer solar cell based on rr-P3HT as the donor for its capability to eliminate interfacial hole traps. This result also reveals the importance of the hole collection layer for the development of highly efficient polymer photovoltaic devices.

From the above discussion, the traps in rr-P3HT can be characterized as interfacial and bulk traps from the present TSC measurements which are illustrated in Figure 4. The interfacial trap is a hole trap with TSC peak maximum at 225 K and locates at the ITO/rr-P3HT interface, which can be eliminated by inserting a layer of PEDOT:PSS. For the bulk trap, its polarity was determined to be hole traps with a TSC maximum of 110 K. Upon exposure of rr-P3HT to O_2, the number of trapped holes can be enhanced and a new deep electron trap (onset of detrapping temperature is about 225 K) is formed. Both traps related to adsorbed O_2 show partial reversibility in their charge trapping capability, suggesting that it is very important to prevent rr-P3HT based devices from O_2 exposure for avoiding any possible degradation in device performance.

Traps in the rr-P3HT:PCBM. The rr-P3HT:PCBM blend is the most investigated model system in polymer solar cells. A deep understanding of traps in this model system can provide a route for development of highly efficient polymer photovoltaic

dx.doi.org/10.1021/am303186f | ACS Appl. Mater. Interfaces 2013, 5, 4086−4092

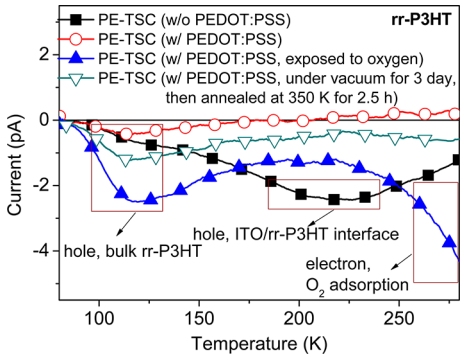

Figure 4. Comparison of PE-TSC spectra of the rr-P3HT device under various experimental conditions.

devices. In the following, traps and their polarities in the rr-P3HT:PCBM blend will be investigated by the TSC measurement. The influence of oxygen exposure and fabrication conditions (annealing process and mixing ratio) on traps in this blend will also be explored.

Figure 5 is the TSC spectra of rr-P3HT:PCBM (1:1 w/w) with various experimental conditions. For comparison

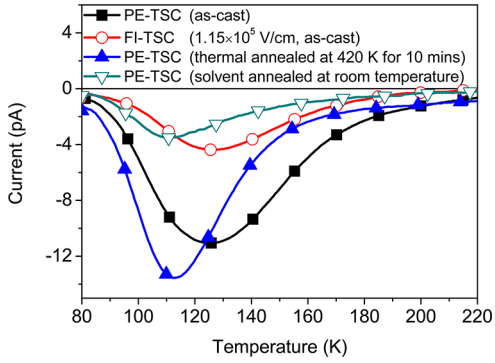

Figure 5. TSC spectra of rr-P3HT:PCBM (1:1 w/w) device under various experimental conditions.

purposes, the PE-TSC of pure PCBM with trap filling at 18 K can also be found in ref 28. The pure PCBM shows a TSC peak between 18 and 160 K with the maximum at about 55 K, indicating distributed trap states, though its polarity was not given. No additional TSC peak was observed up to room temperature. For the fullerene C_{60}, the presence of electron traps from the measurement of an *n*-type organic thin film transistor (OTFT) has been reported.[29] Therefore, it is reasonably to assign the TSC peak in PCBM in ref 28 to a release of trapped electrons from the electron trap. For the nonannealed rr-P3HT:PCBM spin-coated from its solution in CB, it gives a peak ranging from 80 to 220 K with a maximum at 125 K. By comparison of the PE-TSC of as-cast rr-P3HT:PCBM (Figure 5) with PE-TSC of pure rr-P3HT (Figure 1) and fractional TSC of pure PCBM with T_{stop} = 80 K (in ref 28, it gives a broad TSC peak between about 80 and 160 K and peak maximum at 100 K), it reveals an overlap of the TSC spectra of rr-P3HT and PCBM, accompanied with increase in density of trap state at detrapping temperatures greater than 170 K due to the larger TSC current. To understand if the PE-TSC peak at 125 K for rr-P3HT:PCBM is dominated by hole detrapping current in rr-P3HT or electron detrapping current in PCBM, FI-TSC with a positive electric field of 1.15×10^5 V cm^{-1} (equivalent to 1.15 V for a film 100 nm thick) was employed. Since the HOMO and LUMO levels of rr-P3HT and PCBM are 5.2 and 3.8 eV, respectively,[17] along with the work functions of PEDOT:PSS (anode, 5.1 eV) and Al (cathode, 4.3 eV) involved in the device structure, the barrier for hole injection (0.1 eV) from PEDOT:PSS to rr-P3HT is much lower than that for electron injection (0.5 eV) from Al to PCBM, and thus, a significant amount of injected holes accompanyied with a negligible amount of electrons can be expected under this positive electrical field. As shown in Figure 5, similar peak position and distribution can still be observed in FI-TSC, suggesting that the peak in PE-TSC is primary due to hole trap of rr-P3HT. The increase in density of hole trap states at detrapping temperature greater than 170 K compared to pristine films in Figure 5 could be explained as follow. The reduction in ordering in the rr-P3HT chains after blending with PCBM will lower the HOMO level of rr-P3HT and lead to a broad distribution of HOMO level for rr-P3HT,[30] in which more ordered rr-P3HT (with higher HOMO level) can act as hole traps in comparison with less ordered rr-P3HT (with lower HOMO level). As a result, additional hole trap states along with more broader TSC peaks as compared to pure rr-P3HT and PCBM can be observed for nonannealed rr-P3HT:PCBM. Besides, it can be noted that an increase in detrapping current at about 120 K in rr-P3HT:PCBM as compared to pure rr-P3HT, in which the former (11 pA) is larger than the latter (0.4 pA) by a factor of 27.5. This phenomenon could be explained by more efficient trap filling due to promoted excition dissociation induced by PCBM.

When the above device is annealed at 420 K (this thermal annealing temperature is higher than that of rr-P3HT (350 K) since postproduction annealing at 423 K for a BHJ-PSC composed of rr-P3HT:PCBM can give the best PCE;[32] as a result, 420 K was adopted for the rr-P3HT:PCBM device) for 10 min or the blend film is prepared by spin-coating from high-boiling-point ODCB solution and placement in covered glass Petri dishes for 1 h to allow the solvent to dry slowly (this process is termed "solvent annealing"), a more narrow distribution along with shift of the TSC peak to lower temperature (113 K) can be obtained (Figure 5). These phenomena could be interpreted as follows: upon thermal annealing or solvent annealing of the sample, an increased crystallinity of rr-P3HT[2,31−34] relative to that in the untreated device can diminish hole trap states originated from a broad distribution in the HOMO level of rr-P3HT and thus a more narrow TSC peak can be expected.

It has been reported that thermal or solvent annealing of rr-P3HT:PCBM based photovoltaic devices can significantly enhance their efficiency.[2,32] The above experimental results can indirectly address the influence of annealing on the performance as follows: the more narrow TSC distribution along with shift of the TSC peak to lower temperature after annealing of rr-P3HT:PCBM composite film implies that holes generated in the active layer can transport through the active layer more easily and contribute to the device photocurrent. As a result, higher device efficiency can be expected. The improved hole mobility in rr-P3HT:PCBM after annealing also supports the above argument.[2,35]

Effects of the presence of O_2 on the PE-TSC of rr-P3HT:PCBM were also investigated (Figure 6). After exposing the thermally annealed sample to O_2 for 12 h, a slight increase in PE-TSC peak height at 113 K by a factor of 1.25 was observed. Furthermore, the detrapping current at a temperature

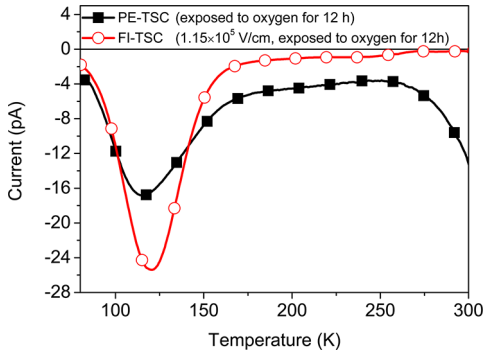

Figure 6. PE-TSC and FI-TSC spectra of a rr-P3HT:PCBM (1:1 w/w) device after exposure to dry O_2 for 12 h.

greater than 250 K in PE-TSC is largely enhanced. However, only one peak at 120 K can be seen from Figure 6 for FI-TSC with positive electric field 1.15×10^5 V cm^{-1} (this peak and the peak at 113 K in PE-TSC in Figure 5 should have the same origin due to the close position); no significant increase in the detrapping current at $T > 250$ K can be observed. The above finding also suggests that the peak at 113 K in PE-TSC is dominated by the hole traps of rr-P3HT. More importantly, as in the case of pure rr-P3HT, additional electron traps with an onset of detrapping temperature at 250 K can be observed in the rr-P3HT:PCBM upon O_2 exposure. Owing to the close onset temperature of detrapping current ($T > 250$ K) and the main chain relaxation of rr-P3HT (230−350 K, Figure 2b), we propose the same electron trap location and detrapping mechanism as in rr-P3HT:O_2 diffusion into the bulk film of rr-P3HT:PCBM which is physically adsorbed to the main chain region of rr-P3HT. When the temperature reaches the relaxation temperatures of the main chain, chain motion starts, promotes O_2 removal, and, consequently, releases the trapped electrons.

Finally, the influence of PCBM content on PE-TSC of rr-P3HT:PCBM was investigated. Figure 7 shows the PE-TSC

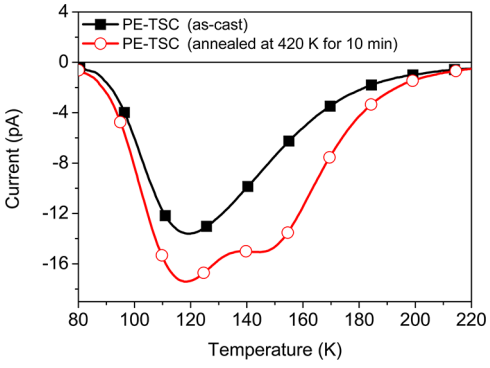

Figure 7. Comparison of PE-TSC spectra of a rr-P3HT:PCBM (4:1 w/w) device before and after thermal annealing treatment at 420 K for 10 min.

spectra of rr-P3HT:PCBM (4:1 w/w) before and after thermal annealing at 420 K for 10 min. In the case of thermally annealed sample, two peaks appear, one located at 118 K and the other at 147 K. However, only one peak (118 K) can be seen from the PE-TSC spectrum of the as-cast sample, which is mainly resulted from detrapping of holes from rr-P3HT due to its peak location close to the peak at 113 K for the rr-P3HT:PCBM (1:1 w/w) in Figure 5. As regards to the higher temperature TSC peak (147 K), we propose the following scenario that explains a formation of the new TSC peak upon thermal treatment. That is: PCBM aggregates are induced by thermal annealing. However, the weight ratio of PCBM to rr-P3HT (1:4 w/w) is relatively low as compared to that in rr-P3HT:PCBM (1:1 w/w) by a factor of 4, leading to much longer spatial distance between PCBM aggregates for the former. When electrons generated by photoexcitation are located at some of PCBM aggregates in rr-P3HT:PCBM (4:1 w/w), it is not easy for the electrons to hop across the active layer via PCBM aggregates, that is, no percolated pathway is formed for electrons. Therefore, the trapping effect related to this insufficient PCBM content can be observed from the TSC spectrum. A PCE value of 1.1% has been reportedly observed in the rr-P3HT:PCBM (4:1 w/w) based solar cell, which is lower than that of rr-P3HT:PCBM (1:1 w/w) (3.75%) by a factor of 3.4.[36] Apart from intuitively ascribing poor performance in rr-P3HT:PCBM (4:1 w/w) to lower probability of exciton dissociation due to lower content PCBM, it should be noted that the fill factor of rr-P3HT:PCBM (4:1 w/w) (42%) is dramatically lower than that of rr-P3HT:PCBM (1:1 w/w) (68%),[36] which is indicative of higher recombination probability,[37] possibly caused by having less percolation paths for transporting electrons to the electrode.

From the above TSC measurement, the rr-P3HT:PCBM blend can give a broad TSC peak (dominated by hole trap of rr-P3HT) ranging from 80 to 220 K with a maximum at 125 K as compared to pure rr-P3HT and pure PCBM. After thermal annealing or solvent annealing of the blend film, more narrow TSC distribution accompanyied by shift of the TSC peak to 113 K can be observed. Similar to rr-P3HT, a new deep electron trap with an onset of detrapping temperature 250 K is observed in the blend upon O_2 exposure. The low content of PCBM in the blend film can also have a trapping effect as evidenced from the new TSC peak located at 147 K. All the above results are illustrated in Figure 8.

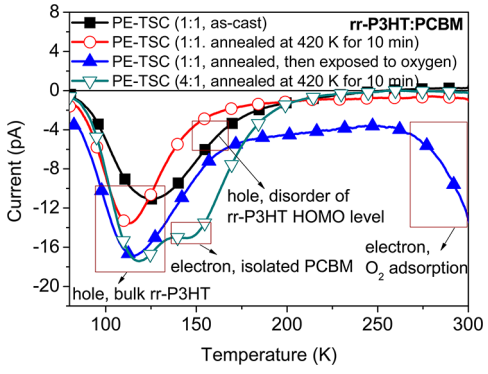

Figure 8. Comparison of PE-TSC spectra of the rr-P3HT:PCBM device under various experimental conditions.

CONCLUSIONS

In conclusion, various traps and their polarities in rr-P3HT and rr-P3HT:PCBM were investigated by the TSC technique. The hole traps located at the ITO/rr-P3HT interface and bulk rr-P3HT are revealed from TSC measurement. Besides, a new deep electron trap with onset of detrapping temperature at about 225 K is characterized in the O_2 exposed rr-P3HT for the first time, and the detrapping process for trapped electrons is strongly related to main chain motion of rr-P3HT. In the blend

dx.doi.org/10.1021/am303186f | ACS Appl. Mater. Interfaces 2013, 5, 4086−4092

of rr-P3HT with PCBM, both thermal and solvent annealing processes and blend ratio can have a significant effect on trap distribution, which is not reported previously. Besides, electron traps related to the presence of O_2 can still be observed in the blend system. We believe that investigations on these important aspects will provide a guideline for molecular design and device fabrication processes and optimized device performances can be achieved.

AUTHOR INFORMATION

Corresponding Author

*Tel.: 886-3-5710733. Fax: 886-3-5737798. E-mail: sachen@che.nthu.edu.tw.

Notes

The authors declare no competing financial interest.

ACKNOWLEDGMENTS

The authors thank the National Science Council for financial support through Project NSC 99-2120-M-007-012 and NSC 100-2120-M-007-009.

REFERENCES

(1) He, Z.; Zhong, C.; Su, S.; Xu, M.; Wu, H.; Cao, Y. *Nat. Photon.* **2012**, *6*, 593−597.
(2) Li, G.; Shrotriya, V.; Huang, J.; Yao, Y.; Yang, Y. *Nat. Mater.* **2005**, *4*, 864−868.
(3) Reyes-Reyes, M.; Kim, K.; Dewald, J.; Lopez-Sandoval, R.; Avadhanula, A.; Curran, S.; Carroll, D. L. *Org. Lett.* **2005**, *7*, 5749−5752.
(4) Coakley, K. M.; McGehee, M. D. *Chem. Mater.* **2004**, *16*, 4533−4542.
(5) Malm, N. V.; Steiger, J.; Schmechel, R.; Seggern, H. V. *J. Appl. Phys.* **2001**, *89*, 5559−5563.
(6) Malm, N. V.; Steiger, J.; Heil, H.; Schmechel, R.; Seggern, H. V. *J. Appl. Phys.* **2002**, *92*, 7564−7570.
(7) Meier, M.; Karg, S.; Zuleeg, K.; Brutting, W.; Schwoerer, M. *J. Appl. Phys.* **1998**, *84*, 87−92.
(8) Alagiriswamy, A. A.; Narayan, K. S. *Synth. Met.* **2001**, *116*, 297−299.
(9) Stallinga, P.; Gomes, H. L.; Rost, H.; Holmes, A. B.; Harrison, M. G.; Friend, R. H.; Biscarini, F.; Taliani, C.; Jones, G. W.; Taylor, D. M. *Phys. B* **1999**, *273*, 923−926.
(10) Schafferhans, J.; Baumann, A.; Deibel, C.; Dyakonov, V. *Appl. Phys. Lett.* **2008**, *93*, 093303.
(11) Nikitenko, V. R.; Heil, H.; von Seggern, H. *J. Appl. Phys.* **2003**, *94*, 2480−2485.
(12) Schafferhans, J.; Baumann, A.; Wagenpfahl, A.; Deibel, C.; Dyakonov, V. *Org. Electron.* **2010**, *11*, 1693−1700.
(13) Baumann, A.; Savenije, T. J.; Murthy, D. H. K.; Heeney, M.; Dyakonov, V.; Carsten, Deibel. *Adv. Funct. Mater.* **2011**, *21*, 1687−1692.
(14) Kawano, K.; Adachi, C. *Adv. Funct. Mater.* **2009**, *19*, 3934−3040.
(15) Frenkel, J. *Phys. Rev.* **1938**, *54*, 647−648.
(16) Fang, Z.; Shan, L.; Schlesinger, T. E.; Milnes, A. G. *Mater. Sci. Eng., B* **1990**, *5*, 397−408.
(17) Ke, W. J.; Lin, G. H.; Hsu, C. P.; Chen, C. M.; Cheng, Y. S.; Jen, T. H.; Chen, S. A. *J. Mater. Chem.* **2011**, *21*, 13483−13489.
(18) Hsieh, C. H.; Cheng, Y. J.; Li, P. J.; Chen, C. H.; Martin, D.; Liang, R. M.; Hsu, C. S. *J. Am. Chem. Soc.* **2010**, *132*, 4887−4893.
(19) Nardes, A. M.; Kemerink, M.; de Kok, M. M.; Vinken, E.; Maturova, K.; Janssen, R. A. J. *Org. Electron.* **2008**, *9*, 727−734.
(20) Narioka, S.; Ishii, H.; Yoshimura, D.; Sei, M.; Ouchi, Y.; Seki, K.; Hasegawa, S.; Miyazaki, T.; Harima, Y.; Yamashita, K. *Appl. Phys. Lett.* **1995**, *67*, 1899−1901.
(21) Tseng, H. E.; Peng, K. Y.; Chen, S. A. *Appl. Phys. Lett.* **2003**, *82*, 4086−4088.
(22) Tseng, H. E.; Liu, C. Y.; Chen, S. A. *Appl. Phys. Lett.* **2006**, *88*, 042112.
(23) Chen, S. A.; Liao, C. S. *Macromolecules* **1993**, *26*, 2810−2816.
(24) Dudognon, E.; Bernes, A.; Lacabanne, C. *Macromolecules* **2001**, *34*, 3988−3992.
(25) Sauer, B. B.; Kim, Y. H. *Macromolecules* **1997**, *30*, 3323−3328.
(26) Correia, N. T.; Alvarez, C.; M Ramos, J. J. *J. Phys. Chem. B* **2001**, *105*, 5663−5669.
(27) Choulis, S. A.; Kim, Y.; Nelson, J.; Bradley, D. D. C.; Giles, M.; Shkunov, M.; McCulloch, I. *Appl. Phys. Lett.* **2004**, *85*, 3890−3892.
(28) Schafferhans, J.; Deibel, C.; Dyakonov, V. *Adv. Energy Mater.* **2011**, *1*, 655−660.
(29) Matsushima, T.; Yahiro, M.; Adachi, C. *Appl. Phys. Lett.* **2007**, *91*, 103505.
(30) Tsoi, W. C.; Spencer, S. J.; Yang, L.; Ballantyne, A. M.; Nicholson, P. G.; Turnbull, A.; Shard, A. G.; Murphy, C. E.; Bradley, D. D. C.; Nelson, J.; Kim, J.-S. *Macromolecules* **2011**, *44*, 2944−2952.
(31) Padinger, F.; Rittberger, R. S.; Sariciftci, N. S. *Adv. Funct. Mater.* **2003**, *13*, 85−88.
(32) Ma, W.; Yang, C.; Gong, X.; Lee, K.; Heeger, A. J. *Adv. Funct. Mater.* **2005**, *15*, 1617−1622.
(33) Zhokhavets, U.; Erb, T.; Hoppe, H.; Gobsch, G.; Sariciftci, N. S. *Thin Solid Films* **2006**, *496*, 679−682.
(34) Marsh, R. A.; Hodgkiss, J. M.; Albert-Seifried, S.; Friend, R. H. *Nano Lett.* **2010**, *10*, 923−930.
(35) Mihailetchi, V. D.; Xie, H. X.; de Boer, B.; Koster, L. J. A.; Blom, P. W. M. *Adv. Funct. Mater.* **2006**, *16*, 699−708.
(36) Kumar, A.; Devine, R.; Mayberry, C.; Lei, B.; Li, G.; Yang, Y. *Adv. Funct. Mater.* **2010**, *20*, 2729−2736.
(37) Servaites, J. D.; Ratner, M. A.; Marks, T. J. *Energy Environ. Sci.* **2011**, *4*, 4410−4422.